Tracking Error-Based Servohydraulic Actuator Adaptive Compensation for Real-Time Hybrid Simulation

Cheng Chen[1] and James M. Ricles[2]

Abstract: Real-time hybrid simulation combines experimental testing and numerical simulation by dividing a structural system into experimental and analytical substructures. Servohydraulic actuators are typically used in a real-time hybrid simulation to apply command displacements to the experimental substructure(s). Servohydraulic actuators may develop a time delay due to inherent actuator dynamics that results in a desynchronization between the measured restoring force(s) and the integration algorithm in a real-time hybrid simulation. Inaccuracy or even instability will occur in a hybrid simulation if actuator delay is not compensated properly. This paper presents an adaptive compensation method for actuator delay. An adaptive control law is developed using an error tracking indicator to adapt a compensation parameter used in the proposed compensation method. Laboratory tests involving large-scale real-time hybrid simulations of a single degree of freedom moment resisting frame with an elastomeric damper are conducted to experimentally demonstrate the effectiveness of the proposed adaptive compensation method. The actuator tracking capability is shown to be greatly improved and exceptional experimental results are still achieved when a good estimate of actuator delay is not available.

DOI: 10.1061/(ASCE)ST.1943-541X.0000124

CE Database subject headings: Experimentation; Hybrid methods; Monitoring; Substructures; Adaptive systems.

Author keywords: Experimentation; Hybrid methods; Tracking; Compensation; Adaptive systems.

Introduction

Hybrid simulation is an experimental method which examines the dynamic response of structures using a hybrid model comprised of both experimental (physical) and analytical (numerical) substructures. The coupling between the substructures is achieved by maintaining the compatibility and equilibrium at the interfaces between the substructures. Hybrid simulation therefore provides a viable alternative for large- or full-scale testing of a civil engineering structure when it is difficult or uneconomical to test the structure on a shaking table. In a hybrid simulation the structural response is solved within a time step using a numerical integration algorithm for a specified external excitation. Command displacements are generated based on the computed structural response and applied to the experimental and numerical substructures. The restoring forces of the substructures are feed back to the integration algorithm for the next time step calculation of structural response. The experimental and analytical substructures, the integration algorithm and the servohydraulic actuator(s) combine together to form a hybrid simulation system.

Many load rate dependent seismic devices have recently been developed to enhance the seismic performance of structural systems during an earthquake (Soong and Spencer 2002; Lee et al. 2005). The development of performance-based design procedures for structures with these devices requires that the performance of the structural system with the devices be evaluated and the design procedure be verified by conducting tests at a real-time scale. Real-time hybrid simulation presents itself as a useful experimental technique to achieve these requirements in an economical and effective manner.

Unlike conventional hybrid simulation (Dermitzakis and Mahin 1985), the command displacements in a real-time hybrid simulation are imposed by the servohydraulic actuator(s) at a real-time scale. Due to inherent servohydraulic dynamics, a time delay can be introduced between the time that an actuator receives the displacement command and when the actuator reaches the desired position, resulting in desynchronization between the measured restoring force(s) for the experimental substructure(s) and the integration algorithm. This delay is usually referred to as actuator delay. The effect of actuator delay for real-time hybrid simulation has been investigated by numerous researchers (Nakashima et al. 1992; Horiuchi et al. 1999; Blakeborough et al. 2001). Wallace et al. (2005a) and Mercan and Ricles (2007) performed stability analysis of real-time hybrid simulation using a delay differential equation when actuator delay exists in the feedback restoring force from the experimental substructure. Chen and Ricles (2008c) introduced discrete control theory to include an explicit integration algorithm in the stability analysis and investigated the effect of actuator delay on real-time hybrid simulation. These studies show that actuator delay will destabilize the real-time simulation if not compensated properly.

Several on-line error indicators have been developed by researchers associated with actuator control error in a real-time hybrid simulation, including the hybrid simulation energy monitor (HSEM) by Mosqueda et al. (2007a,b) and the tracking indicator (TI) by Mercan (2007). In the HSEM procedure, the error indica-

[1]Assistant Professor, School of Engineering, San Francisco State Univ., San Francisco, CA 94132 (corresponding author). E-mail: chcsfsu@sfsu.edu

[2]Bruce G. Johnston Professor, ATLSS Research Center, Dept. of Civil and Environmental Engineering, Lehigh Univ., Bethlehem, PA 18015. E-mail: jmr5@lehigh.edu

Note. This manuscript was submitted on October 7, 2008; approved on September 7, 2009; published online on March 15, 2010. Discussion period open until September 1, 2010; separate discussions must be submitted for individual papers. This paper is part of the ***Journal of Structural Engineering***, Vol. 136, No. 4, April 1, 2010. ©ASCE, ISSN 0733-9445/2010/4-432–440/$25.00.

tor is based on the accumulative energy error in the experimental substructure(s) due to actuator delay, while in the TI procedure, the error indicator is based on the actuator tracking error. Both the HSEM and the TI provide some insight into quality of the real-time hybrid simulation result.

Actuator delay compensation is used in real-time hybrid simulation to minimize the effect of actuator delay by achieving accurate actuator control. Various compensation methods have been proposed for real-time hybrid simulation. Horiuchi et al. (1999) and Horiuchi and Konno (2001) proposed two compensation schemes, the first based on a polynomial extrapolation and the second based on an assumption of linear structural acceleration, respectively. Carrion and Spencer (2006) modified Horiuchi's method to include structural properties and the external excitation force. Other compensation methods have originated from control theory, where the servohydraulic system is treated as a time delay system and delay compensation methods, such as phase lead compensator (Zhao et al. 2003) and derivative feedforward (Jung and Shing 2006; Jung et al. 2007; Mercan 2007) are introduced. Other methods used for actuator delay compensation in real-time hybrid simulation include the Smith Predictor (Shao et al. 2006) and the virtual coupling method (Christenson et al. 2008). Chen (2007) proposed a simplified model for servohydraulic actuator response using a first order discrete transfer function, and applied the inverse of the model's transfer function to compensate for actuator delay in a real-time hybrid simulation. This compensation is referred to as the inverse compensation method.

The aforementioned compensation methods are developed for a constant actuator delay. Applying these compensation methods in real-time hybrid simulation requires an accurate estimate of actuator delay. Accurately estimating an actuator delay can be difficult in actual practice. Moreover, the actuator delay might vary during the simulation due to the nonlinearities in the experimental substructure and the servohydraulic system.

Compensation methods based on adaptive control theory have also been developed. Darby et al. (1999) proposed an on-line procedure to estimate and compensate for actuator delay during a real-time hybrid simulation. Wallace et al. (2005b) proposed an adaptive controller with on-line prediction to minimize the delay error in a servohydraulic system. Bonnet et al. (2007) applied the model reference adaptive minimal control synthesis for actuator control in real-time hybrid simulation. Ahmadizadeh et al. (2008) modified the delay estimation algorithm developed by Darby et al. (1999) by incorporating into it a linear acceleration extrapolation scheme to minimize the effect of variable actuator delay.

In this paper an adaptive compensation method is developed to achieve accurate actuator control in real-time hybrid simulation. The formulation for the method is based on using inverse compensation with an adaptable model parameter. The method is referred to as the adaptive inverse compensation method. An adaptive control law based on actuator displacement tracking error is developed to adapt the compensation parameter in the model to minimize the effect of an inaccurately estimated or a time-varying actuator delay in a real-time hybrid simulation. The proposed adaptive compensation method is experimentally evaluated by large-scale real-time hybrid simulations of a single degree of freedom (SDOF) moment resisting frame (MRF) with an elastomeric damper. Actuator control is shown to be significantly improved using the adaptive inverse compensation method, even with a poorly estimated actuator delay, and can thereby enable a reliable real-time hybrid simulation to be achieved. Energy errors resulting from servohydraulic actuator tracking errors (Mosqueda et al. 2007a,b) are used to demonstrate the effectiveness of the proposed adaptive scheme by monitoring the energy balance in a real-time hybrid simulation.

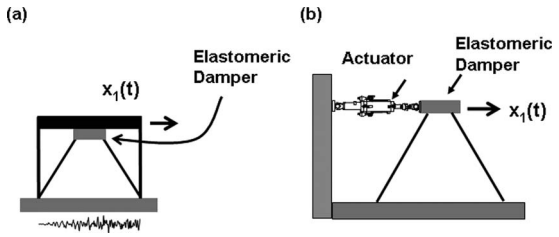

Fig. 1. (a) SDOF with elastomeric damper; (b) experimental substructure

Actuator Delay Modeling and Inverse Compensation

For the real-time hybrid simulation of the SDOF structural model shown in Fig. 1 the equation of motion can be written as

$$m \cdot \ddot{x}(t) + c \cdot \dot{x}(t) + r^a(t) + r^e(t) = F(t) \tag{1a}$$

where m and c=mass and the inherent viscous damping of the structure, respectively; $\dot{x}(t)$ and $\ddot{x}(t)$=velocity and acceleration responses of the structure, respectively; $F(t)$=predefined external excitation force; and $r^a(t)$ and $r^e(t)$=restoring forces of the analytical substructure (i.e., the MRF) and the experimental substructure (i.e., the elastomeric damper), respectively. For linear elastic substructures, the restoring forces can be expressed as $r^a(t) = k_a \cdot x(t)$ and $r^e(t) = k_e \cdot x(t)$, where k_e and k_a are the linear elastic stiffness of the experimental and analytical substructures, respectively, and $x(t)$ is the displacement response of the SDOF structure.

A numerical integration algorithm is usually used in a real-time hybrid simulation to solve the temporally discretized form of Eq. (1*a*), which can be expressed as

$$m \cdot \ddot{x}_{i+1} + c \cdot \dot{x}_{i+1} + r^a_{i+1} + r^e_{i+1} = F_{i+1} \tag{1b}$$

where $\ddot{x}_{i+1}$, $\dot{x}_{i+1}$, and F_{i+1}=acceleration, velocity, and excitation force at time step $i+1$, respectively, and r^e_{i+1} and r^a_{i+1}=restoring forces of the experimental and analytical substructures at time step $i+1$, respectively. The displacement response x_{i+1} determined by the integration algorithm is imposed as a command displacement to the substructures. For the SDOF structure discussed in this paper (as shown in Fig. 1), the command displacements for experimental and analytical substructures at time step $i+1$ are the same as x_{i+1} of the SDOF structure at time step $i+1$.

The command displacement x_{i+1} for the experimental substructure is usually imposed using a servohydraulic actuator. To ensure a smooth actuator response and reduce possible actuator displacement overshoot, a ramp generator is used to interpolate the command displacement x_{i+1} over the integration time step Δt. The time step Δt is typically an integer multiple of the servocontroller sampling time δt For a linear ramp generator, the command displacement sent to the servocontroller is interpolated as

$$d^{c(j)}_{i+1} = \frac{j}{n} \cdot (x_{i+1} - x_i) + x_i \tag{2}$$

In Eq. (2) j is the substep index for the interpolation substep of the ramp generator within the time step and ranges from 1 to n, where n is the integer ratio of $\Delta t / \delta t$. $d^{c(j)}_{i+1}$ in Eq. (2) is the displacement command for the servohydraulic actuator at the jth

J. Struct. Eng., 2010, 136(4): 432-440

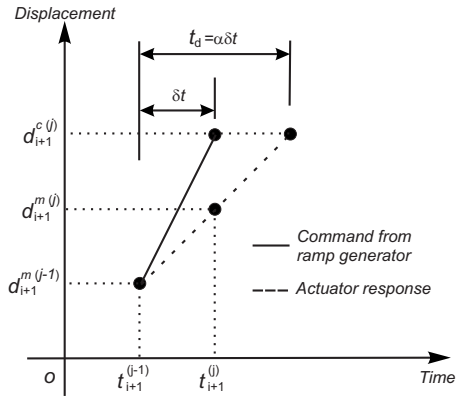

Fig. 2. Actuator response under time delay

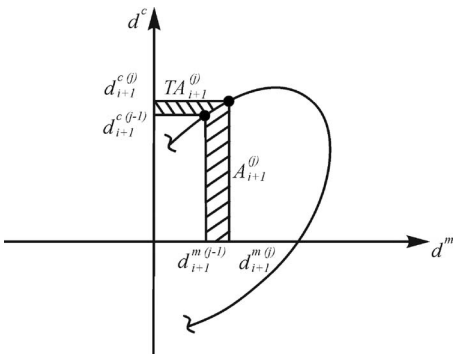

Fig. 3. Definition of TI

substep of the $(i+1)$th time step. Eq. (2) can be modified when other forms of ramp generators are used for real-time hybrid simulation (e.g., a quadratic ramp generator).

Due to servohydraulic dynamics that results in actuator delay, the servohydraulic actuator would reach a delayed measured response $d_{i+1}^{m(j)}$ instead of the command displacement $d_{i+1}^{c(j)}$. For a time interval of δt, which is typically 1/1,024 s for state-of-the-art servocontrollers, the actuator response can be idealized as a linear response, as shown in Fig. 2. The duration for the actuator to achieve the command displacement $d_{i+1}^{c(j)}$ is t_d and designated as $\alpha\delta t$. α is greater than 1.0 when a time delay exists in the actuator response. Assuming that the actuator achieves the measured displacement $d_{i+1}^{m(j-1)}$ at the end of the $(j-1)$th substep during the $(i+1)$th integration time step (which may not be equal to the command displacement $d_{i+1}^{c(j-1)}$), and using the linear actuator response shown in Fig. 2, the measured displacement response $d_{i+1}^{m(j)}$ at the end of the jth substep of the $(i+1)$th time step can be expressed as

$$d_{i+1}^{m(j)} = d_{i+1}^{m(j-1)} + \frac{1}{\alpha} \cdot (d_{i+1}^{c(j)} - d_{i+1}^{m(j-1)}) \tag{3}$$

Applying the discrete z transform (Ogata 1995; Franklin et al. 2002) to Eq. (3) leads to a discrete transfer function $G_d(z)$ relating the measured actuator response $d_{i+1}^{m(j)}$ to the command displacement $d_{i+1}^{c(j)}$, where

$$G_d(z) = \frac{X^m(z)}{X^c(z)} = \frac{z}{\alpha \cdot z - (\alpha - 1)} \tag{4}$$

In Eq. (4), z is the complex variable in discrete z domain, and $X^m(z)$ and $X^c(z)$ are the discrete z transforms of $d_{i+1}^{m(j)}$ and $d_{i+1}^{c(j)}$, respectively.

Chen (2007) proposed to use the inverse of the simplified actuator delay model in Eq. (4) for actuator delay compensation to achieve accurate actuator control in a real-time simulation. The discrete transfer function for the resulting inverse compensation method can be written as

$$G_c(z) = \frac{X^p(z)}{X^c(z)} = \frac{\alpha \cdot z - (\alpha - 1)}{z} \tag{5a}$$

where $X^p(z)$=discrete z transform of the predicted displacement $d_{i+1}^{p(j)}$ to be sent to the servohydraulic actuator controller to compensate for actuator delay associated with the value of α for the jth substep at time step $i+1$ in a real-time simulation.

Applying the inverse discrete z transform to Eq. (5*a*), Chen and Ricles (2008b) showed that the inverse compensation method in the time domain can be expressed as

$$d_{i+1}^{p(j)} = \alpha \cdot d_{i+1}^{c(j)} - (\alpha - 1) \cdot d_{i+1}^{c(j-1)} \tag{5b}$$

Eq. (5*b*) indicates that the inverse compensation method can be interpreted as an extrapolation using the command displacements $d_{i+1}^{c(j-1)}$ and $d_{i+1}^{c(j)}$ in the time domain. Chen et al. (2009) applied inverse compensation to the real-time hybrid simulation of structures with an elastomeric damper. Good actuator tracking was observed when an accurate value of α was used.

Adaptive Inverse Compensation Formulation

An accurate estimate of actuator delay, i.e., the value of α in Eq. (5*a*), may not be available when attempting to use the inverse compensation method for a real-time hybrid simulation. This may also occur to other actuator delay compensation methods such as the linear acceleration extrapolation method and derivative feedforward compensation method, leading to under- or overcompensation.

To minimize the effect of an inaccurately estimated actuator delay for a real-time hybrid simulation, an adaptive inverse compensation method is therefore developed in this paper. The formulation is based on Eq. (5*a*) with an adaptive parameter, where

$$G_c(z) = \frac{X^p(z)}{X^c(z)} = \frac{(\alpha_{es} + \Delta\alpha) \cdot z - (\alpha_{es} + \Delta\alpha - 1)}{z} \tag{6}$$

In Eq. (6) α_{es} is the estimated actuator delay and $\Delta\alpha$ is an evolutionary variable (i.e., adaptive parameter) for the adaptive inverse compensation method. An adaptive control law is used to determine $\Delta\alpha$ that is based on the TI described in the following, where $\Delta\alpha$ is defined as

$$\Delta\alpha(t) = k_p \cdot \mathrm{TI}(t) + k_i \cdot \int_0^t \mathrm{TI}(\tau)dt \tag{7}$$

In Eq. (7) k_p and k_i are proportional and integrative adaptive gains of the adaptive control law, respectively, and $\Delta\alpha$ has an initial value of zero. The TI is based on the enclosed area of the hysteresis in the synchronized subspace plot shown in Fig. 3, where the actuator command displacement $d_{i+1}^{c(j)}$ is plotted against the actuator measured response $d_{i+1}^{m(j)}$. The calculation of TI at each time step is formulated as (Mercan 2007)

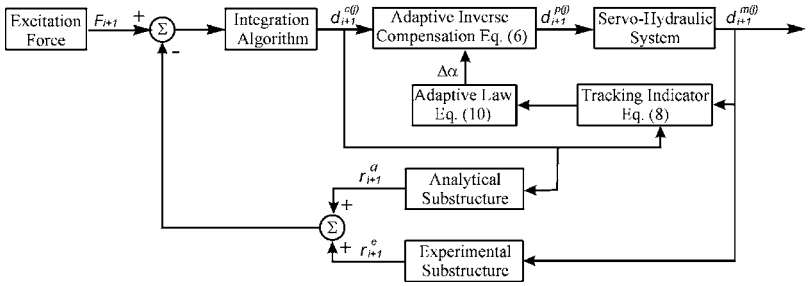

Fig. 4. Schematic implementation of adaptive compensation

$$TI_{i+1}^{(j)} = 0.5(A_{i+1}^{(j)} - TA_{i+1}^{(j)}) \tag{8}$$

In Eq. (8), $A_{i+1}^{(j)}$ and $TA_{i+1}^{(j)}$ are the enclosed and complementary enclosed areas for the jth substep of the ramp generator at time step $i+1$, respectively, as shown in Fig. 3, and are calculated as

$$A_{i+1}^{(j)} = A_{i+1}^{(j-1)} + 0.5(d_{i+1}^{c(j)} + d_{i+1}^{c(j-1)})(d_{i+1}^{m(j)} - d_{i+1}^{m(j-1)}) \tag{9a}$$

$$TA_{i+1}^{(j)} = TA_{i+1}^{(j-1)} + 0.5(d_{i+1}^{m(j)} + d_{i+1}^{m(j-1)})(d_{i+1}^{c(j)} - d_{i+1}^{c(j-1)}) \tag{9b}$$

At the beginning of the test, the enclosed and complementary areas have initial values of zero. The calculation of A and TA continues for every substep of each time step until the end of the real-time hybrid simulation.

Mercan (2007) showed that a positive rate of change of the TI corresponds to an actuator response lagging behind the command displacement, where energy is introduced into the real-time hybrid simulation, while a negative rate of change indicates a leading actuator response, where artificial damping is added into the real-time simulation. A zero rate of change of the TI implies no actuator control error, i.e., the actuator measured and command displacements are equal to each other. When the value of the TI remains equal to zero throughout the simulation, perfect actuator control has been achieved in the real-time hybrid simulation. A variable rate of change of the TI indicates an actuator response with a variable delay (Mercan 2007).

When the adaptive control law in Eq. (7) is used in a real-time hybrid simulation, a lagging actuator response that leads to a positive value for the TI results in a positive value of $\Delta\alpha$ and an increase in the compensation parameter α. A leading actuator response that leads to a negative value for the TI results in a negative value of $\Delta\alpha$ and a decrease in the compensation parameter α.

Eq. (7) gives the adaptation of $\Delta\alpha$ in continuous form. For the purpose of implementation, Eq. (7) needs to be expressed in discrete form, which is

$$\Delta\alpha(z) = k_p \cdot \mathrm{TI}(z) + k_i \cdot \frac{\delta t}{z-1} \times \mathrm{TI}(z) \tag{10}$$

where $\Delta\alpha(z)$ and $TI(z)$=discrete z transforms of $\Delta\alpha$ and the TI, respectively. It can be observed that the adaptation of $\Delta\alpha$ in Eq. (10) depends on the values of k_p and k_i. Generally, a larger value of k_p results in a faster response and a larger oscillation of the evolutionary variable $\Delta\alpha$, while increasing the integration gain k_i reduces the oscillation. The values for k_p and the ratio between k_i and k_p are determined from numerical simulations involving a predefined displacement and the simplified servohydraulic model. The value of k_i/k_p=0.1 is used in the experiments presented in this paper to achieve fast adaptation with only a small and acceptable amount of overshoot. As noted next, a value for k_p=0.4 leads to a fast convergence rate while also maintaining the stability of the servohydraulic system. Fig. 4 shows the schematic representation of the adaptive inverse compensation method for real-time hybrid simulation that was implemented into the real-time integrated control system at the NEES real-time multidirectional facility at Lehigh University (Mercan and Ricles 2008). The integrated control system includes the integration algorithm, the adaptive inverse compensation and the analytical substructure, and is developed and compiled using SIMULINK and Mathworks xPC Target software (MATLAB 2007).

Real-Time Hybrid Simulation Laboratory Tests with Adaptive Inverse Compensation

To experimentally evaluate the performance of the proposed adaptive inverse compensation method, laboratory tests involving large-scale real-time hybrid simulations are conducted at the NEES equipment site at Lehigh University using the SDOF MRF with an elastomeric damper shown in Fig. 1. The SDOF MRF (without the elastomeric damper) has a mass of 503.4 t, an elastic natural frequency of 0.77 Hz, and an inherent viscous damping ratio ζ of 0.02. Fig. 5 shows the experimental setup, which consists of the experimental substructure (elastomeric damper), servohydraulic actuator with a support and roller bearings, and two reaction frames. The elastomeric damper is manufactured from a Butyl blend of rubber and has the characteristics of an elastomeric material at small deformation amplitudes, with friction dominating the behavior at larger amplitudes (Kontopanos 2006). The stiffness K' and loss factor η of the elastomeric material as a function of excitation frequency and deformation amplitude are shown in Fig. 6. K' is the secant stiffness of the damper corresponding to the maximum deformation within a hysteretic loop developed under constant amplitude of imposed deformation. The loss factor η is related to the energy dissipation of the damper per cycle of deformation, and the equivalent viscous damping ξ_{eqiuv} for the damper is equal to 0.5η. The stiffness K' is shown in Fig. 6(a) to be more frequency dependent at smaller deformation amplitudes compared to larger damper deformations. The loss factor is shown in Fig. 6(b) to be frequency dependent, ranging from 0.4

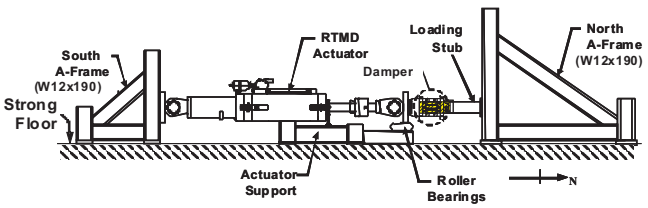

Fig. 5. Schematic of elastomeric damper in test setup for experimental substructure

J. Struct. Eng., 2010, 136(4): 432-440

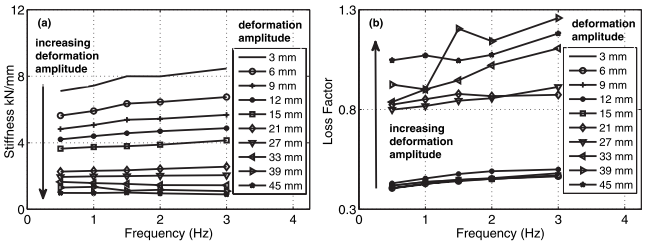

Fig. 6. Elastomeric damper mechanical properties for (a) stiffness K'; (b) loss factor η at room temperature

to 0.5 at small deformations, with a significant increase in η at larger deformations to a value of 1.2 due to the frictional effects. The overall equivalent viscous damping of the system (MRF and damper) is 0.18. The actuator in the experimental setup imposes the interstory displacement to the damper, where the axial stiffness of the loading stub represents the horizontal stiffness of the diagonal braces in the structure. Lee et al. (2005) showed that for a typical MRF with elastomeric dampers, the ratio between the damper stiffness and the brace horizontal stiffness is 20 to 30. Real-time hybrid simulations using the experimental setup in Fig. 5 have been reported by Mercan (2007) and Chen et al. (2009). The servohydraulic actuator controller for the experimental setup consists of a digital PID controller with the proportional gain of 20, integral time constant of 5.0 s resulting in an integral gain of 4.0, differential gain of 0, and a roll-off frequency of 39.8 Hz (Zhang et al. 2005). A large servohydraulic actuator is used in the experimental setup. The actuator has a 1,700-kN maximum force capacity with a 500-mm stroke. Two servovalves, each with a flow capacity of 2,500 gal./min, are mounted on the actuator to give it a maximum velocity capacity of 760 mm/s.

The explicit CR integration algorithm (Chen and Ricles 2008a) is used in the simulation, where the variations of displacement and velocity over the time step are defined as

$$\dot{x}_{i+1} = \dot{x}_i + \Delta t \cdot \alpha_1 \cdot \ddot{x}_i \tag{11a}$$

$$x_{i+1} = x_i + \Delta t \cdot \dot{x}_i + \Delta t^2 \cdot \alpha_2 \cdot \ddot{x}_i \tag{11b}$$

In Eqs. (11*a*) and (11*b*) α_1 and α_2 are integration parameters defined as

$$\alpha_1 = \alpha_2 = \frac{4m}{4 \cdot m + 2 \cdot \Delta t \cdot c + \Delta t^2 \cdot k} \tag{12a}$$

To incorporate the rate-dependent properties of the elastomeric damper in the real-time hybrid simulation, the integration parameters α_1 and α_2 in Eq. (12*a*) are modified as

$$\alpha_1 = \alpha_2 = \frac{4m}{4 \cdot m + 2 \cdot \Delta t \cdot (c + c_{\text{eq}}) + \Delta t^2 \cdot (k_{\text{eq}} + k_a)} \tag{12b}$$

where c_{eq} and k_{eq}=equivalent damping and equivalent stiffness of the elastomeric damper, respectively. The estimated equivalent stiffness and equivalent damping of the elastomeric damper are used to determine the integration parameters of the CR algorithm. Chen et al. (2009) showed that this estimation does not affect the experimental results for the SDOF structure investigated in this paper. The values of k_{eq} and c_{eq} were determined from identification tests performed on the damper and are equal to 7.6 kN/mm and 0.64 kN·s/mm, respectively, for the frequency range and deformation amplitude (story drift) expected to develop in the SDOF system during the real-time hybrid simulation.

The CR integration algorithm in Eqs. (11*a*) and (11*b*) can be observed to be explicit for both the displacement and velocity. Using the discrete transfer function approach, Chen and Ricles (Chen and Ricles 2008a,b) showed that the CR integration algorithm is unconditionally stable for linear elastic structures and for a nonlinear structure with softening behavior. Real-time hybrid simulations using the explicit CR algorithm are reported by Chen et al. (2009). Chen et al. (2009) compared the experimental results with results from experiments using HHT α method with a fixed number of substep iterations (Shing 2002). A good comparison was observed between the results, indicating that the CR algorithm can be used to achieve exceptional and reliable results in a real-time hybrid simulation.

The SDOF MRF, which is the analytical substructure, is modeled using the Bouc-Wen model (Wen 1980), whereby the restoring force of the MRF is defined as

$$r^a(t) = \eta \cdot k_a \cdot x^a(t) + (1 - \eta) \cdot k_a \cdot x_y^a \cdot z(t) \tag{13}$$

In Eq. (13) x_y^a is the yield displacement of the analytical substructure; k_a is the linear elastic stiffness of the analytical substructure; η is the ratio of the post- to preyield stiffness of the analytical substructure; $x^a(t)$ is the displacement imposed on the analytical substructure by the integration algorithm; and $z(t)$ is the evolutionary parameter of the Bouc-Wen model governed by the following differential equation:

$$x_y^a \cdot \dot{z}(t) + \gamma |\dot{x}^a(t)| \cdot z(t) \cdot |z(t)|^{q-1} + \beta \cdot \dot{x}^a(t) \cdot |z(t)|^q - \dot{x}^a(t) = 0 \tag{14}$$

The dimensionless parameters γ, β, and q in Eq. (14) control the shape of the hysteretic loop of the analytical substructure (Wen 1980). The properties of the Bouc-Wen model for the analytical substructure are given in Table 1.

The time step Δt for real-time hybrid simulation is selected as 10/1,024 s, which is 10 times the servocontroller sampling time δt. The N196E component of the 1994 Northridge earthquake recorded at Canoga Park was selected as the ground motion. To ensure a maximum displacement response of less than 30 mm to not damage the damper, the ground motion is scaled to have a maximum magnitude of acceleration of 0.322 m/s^2.

To systematically evaluate the performance of the proposed adaptive compensation method, different values of α_{es}, k_p, and k_i are used in the real-time hybrid simulations. Three different values for the estimated actuator delay constant α_{es} (α_{es}=29, 15, and 45) and three sets of the proportional adaptive gains (k_p=0, 0.2, and 0.4) are used in the real-time hybrid simulations. The case of k_p=0 represents a real-time hybrid simulation using conventional inverse compensation. The value of k_i was always set equal to $0.1k_p$. It was determined from tests with predefined sinusoidal actuator command displacements that a value of α_{es}=29 represents an accurate estimate for actuator delay for the frequency range and actuator displacement expected to occur in the SDOF

Table 1. Values for Parameter of the Bouc-Wen Model for the Analytical Substructure

Parameters	k_a (KN/mm)	η	x_y^a (mm)	β	γ	q
Value	11.76	0.0	10	0.55	0.45	2

J. Struct. Eng., 2010, 136(4): 432-440

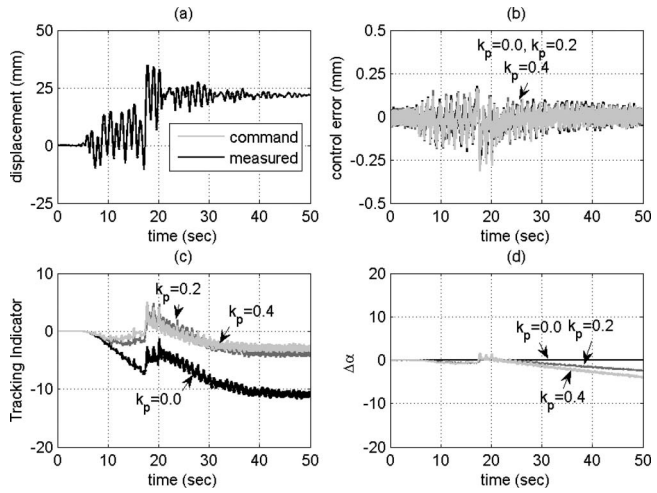

Fig. 7. Real-time hybrid simulation results using adaptive inverse compensation (α_{es}=29): (a) comparison of command displacement and measured actuator response; (b) control error; (c) TI; and (d) time history of $\Delta\alpha$

system during the real-time hybrid simulation. Values of α_{es}=15 and α_{es}=45 correspond to poor estimates of actuator delay for real-time hybrid simulation and represent about a ±50% error in actuator delay estimation.

Real-Time Hybrid Simulation Laboratory Test Results

The real-time hybrid simulation results using adaptive inverse compensation with α_{es} equal to 29 are presented in Fig. 7. The comparison of the command displacement and the measured actuator displacement for the real-time hybrid simulation using adaptive compensation method with k_p=0.4 is presented in Fig. 7(a). Good tracking can be observed. The displacement history has maximum and minimum values of about 34.5 mm and −10.3 mm, respectively. Yielding of the analytical substructure occurred, beginning at around 15 s, leading to a residual drift of 24 mm at the end of the test. The force-deformation responses of the analytical and experimental substructures are presented in Fig. 8. The restoring forces developed in the two substructures are shown to be approximately the same value, whereby the elastomeric damper resisted from 44 to 55% of the story shear of the structure. Energy dissipation is shown to have occurred in both the elastomeric damper and the MRF.

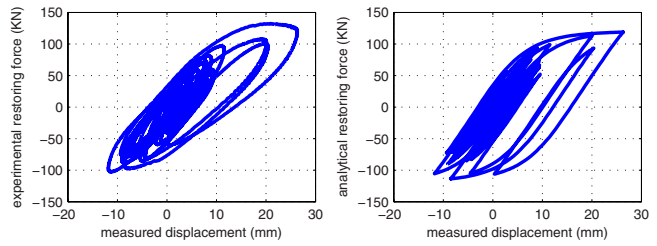

Fig. 8. Hysteresis of analytical and experimental substructures of real-time hybrid simulation using adaptive inverse compensation (α_{es}=29, k_p=0.4, k_i=0.04)

The difference between the command displacement and the actuator measured displacements (referred to as control error) that occurred during the simulation is presented in Fig. 7(b), where the results for the simulations using different values of k_p are shown. The results for k_p=0.2 and k_p=0.4 are nearly identical. A summary of the maximum control errors for the tests discussed earlier is given in Table 2. Also included are the maximum control errors normalized by the maximum actuator command displacements in addition to the *error norm* defined as the RMS of the control error divided by the RMS of the command displacement. The error norm is given by

$$\text{error norm} = \sqrt{\frac{\frac{1}{N}\sum_{i=1}^{N}[d_i^c - d_i^m]^2}{\frac{1}{N}\sum_{i=1}^{N}[d_i^c]^2}} \tag{15}$$

where N=number of time steps in the real-time test.

A maximum magnitude of 0.31 mm, 0.28 mm, and 0.28 mm occurred in the simulations with k_p=0, 0.2, and 0.4, respectively. These maximum control errors correspond to about 0.52%, 0.48%, and 0.47% error, respectively, in the command displacement (see Table 2). The error norm corresponding to these cases are 0.0081, 0.0079, and 0.0079. Fig. 7(c) shows the time history for the TI of the real-time hybrid simulations. The simulation with k_p=0 is observed to have a minimum value of −10, while the two with adaptive compensation (i.e., k_p=0.2 and 0.4) are observed to have the values of the TI equal to almost zero, indicating better actuator tracking for the real-time hybrid simulation is achieved when the proposed adaptive inverse compensation method is used. Fig. 7(d) presents the time history of the evolutionary vari-

Table 2. Maximum Control Error in Real-Time Hybrid Simulations

Case	α_{es}	k_p	Maximum control error (mm)	$\frac{\max \text{ control error}}{\max\lvert d^c\rvert} \times 100$ (%)	Error norm (%)
1	29	0	0.31	0.52	0.81
	29	0.2	0.28	0.48	0.79
	29	0.4	0.28	0.47	0.79
2	15	0	1.55	4.22	1.53
	15	0.2	0.55	1.53	0.54
	15	0.4	0.49	1.36	0.43
3	45	0	1.61	4.58	1.84
	45	0.2	0.58	1.61	0.55
	45	0.4	0.54	1.51	0.49

J. Struct. Eng., 2010, 136(4): 432-440

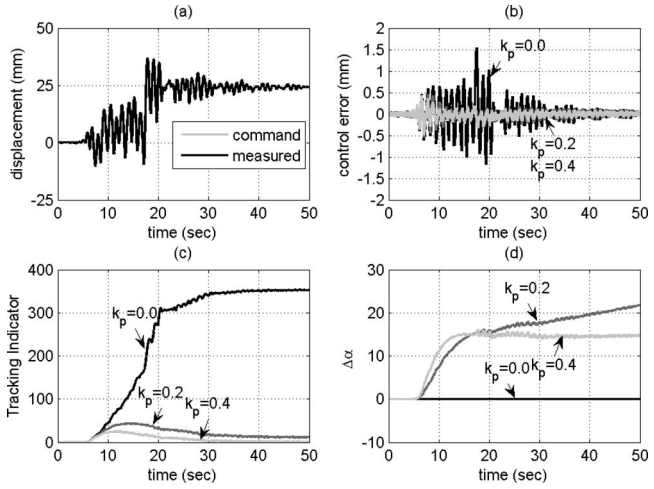

Fig. 9. Real-time hybrid simulation results using adaptive inverse compensation (α_{es}=15): (a) comparison of command displacement and measured actuator response; (b) control error; (c) TI; and (d) time history of $\Delta\alpha$

able $\Delta\alpha$, which can be observed to have a small negative value for k_p=0.2 and 0.4. This implies that the adaptive mechanism adjusted for a slight overcompensation that exists when α_{es} equals 29.

The real-time hybrid simulation results using the proposed adaptive compensation method with α_{es} equal to 15 and 45 are presented in Figs. 9 and 10, respectively. The comparisons of the command displacements and the measured actuator response are presented in Figs. 9(a) and 10(a) for simulations with k_p equal to 0.4, where good tracking can again be observed. The control error between the command displacements and the measured actuator responses are shown in Figs. 9(b) and 10(b), with the maximum control error summarized in Table 2 for different values of k_p. It can be observed that due to the poor estimate of actuator delay, the control errors without adaptive compensation are noticeably larger in Figs. 9(b) and 10(b) than those in Fig. 7(b). The control error is shown in Figs. 9(b) and 10(b) and Table 2 to reduce when

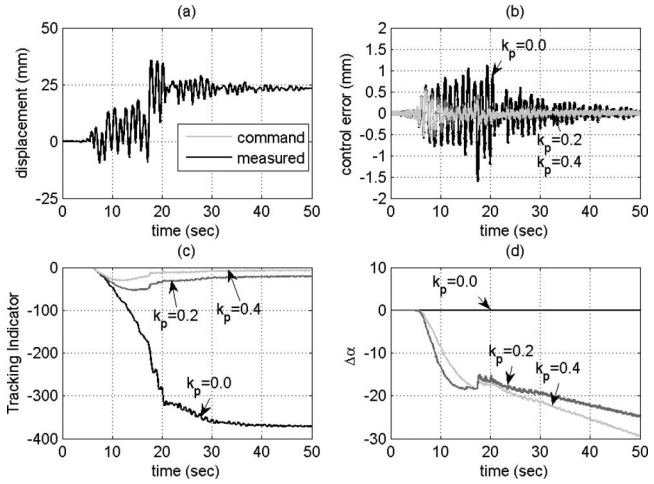

Fig. 10. Real-time hybrid simulation results using adaptive inverse compensation (α_{es}=45): (a) comparison of command displacement and measured actuator response; (b) control error; (c) TI; and (d) time history of $\Delta\alpha$

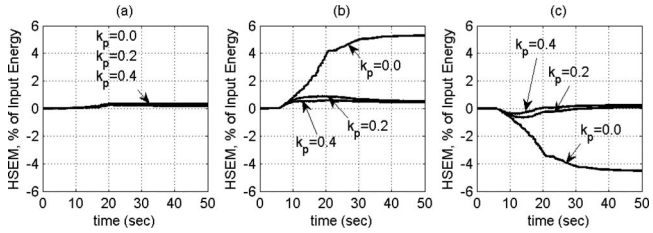

Fig. 11. HSEM of real-time hybrid simulation results with adaptive inverse compensation: (a) α_{es}=29; (b) α_{es}=15; and (c) α_{es}=45

adaptive inverse compensation is used (i.e., when k_p=0.2 and 0.4). The simulation with k_p=0.4 has the smallest control error for all the simulations, with the maximum magnitude of control error equal to 0.49 mm, and 0.54 mm for α_{es}=15 and α_{es}=45, respectively (see Table 2). These errors correspond to 1.36% and 1.51% of the maximum magnitude of the command displacement, as given in Table 2. The values of the error norm corresponding to these cases are 0.0043 and 0.0049. The values of the TIs for the simulations are presented in Figs. 9(c) and 10(c). It can be observed that simulations with adaptive compensation have significantly smaller values for the TI compared to simulations that do not utilize adaptive compensation (i.e., simulations with k_p=0). The TI in Fig. 9(c) increases initially due to the underestimation of actuator delay (i.e., α_{es}=15) and then decreases when the adaptive compensation takes effect. On the contrary, Fig. 10(c) shows an initial decrease of the TI due to the overestimation of actuator delay (i.e., α_{es}=45) and then the TI approaches zero because of the adaptive compensation. The varying slope in the TI history for the cases when k_p=0.0 in Figs. 9(c) and 10(c) indicates the strong presence of a noticeable variable actuator delay. The adaptations of the evolutionary variable $\Delta\alpha$ for the real-time hybrid simulations are presented in Figs. 9(d) and 10(d). The adaptive mechanism is shown to make notable adjustments in the inverse compensation parameter beginning at around 6 s, when the actuator command displacements begin to become large.

It can be observed from Table 2 that for the cases of α_{es}=15 and α_{es}=45 that the adaptive inverse compensation significantly reduces the error norm of the actuator control, leading to accurate actuator control in the real-time hybrid simulation. It can also be observed that with the adaptive gain k_p increased from 0.2 to 0.4, the error norm has almost the same value. It was found that increasing the value of k_p beyond 0.4 will not significantly improve the actuator control. The accuracy of temposonic sensor used to measure actuator displacement is $\pm$0.5 mm. Comparing the maximum control error in Table 2, it can be observed that differences in this error between cases with an estimated delay of 29, 15, and 45 are within 0.5 mm when the adaptive compensation (i.e., k_p=0.2 or 0.4) is used. Hence, for the various cases with different estimated delay the same results are achieved within the accuracy of the testing equipment.

The HSEM (Mosqueda et al. 2007a,b) is also used to evaluate the performance of test results obtained using the proposed adaptive inverse compensation method and is presented in Fig. 11. For simulations with a good estimate of actuator delay, Fig. 11(a) shows that HSEM is less than 1% of the input energy. For simulations with poor estimates and without adaptive compensation (i.e., k_p=0), the HSEM is shown in Figs. 11(b and c) to be around 6% and −6% for the cases with α_{es}=15 and α_{es}=45, respectively; while for simulations with adaptive compensation (i.e., k_p=0.2 and 0.4), the magnitude of the HSEM is reduced to around 1% for the cases with α_{es}=15 and α_{es}=45. The smaller magnitudes for

J. Struct. Eng., 2010, 136(4): 432-440

the HSEM for the simulations with a poorly estimated actuator delay further indicate the effectiveness of the proposed adaptive inverse compensation method in compensating for actuator delay.

The application of the proposed adaptive inverse compensation method requires establishing the value of the proportional gain k_p, which is likely specific to the servohydraulic equipment used in a real-time hybrid simulation. The optimal value of the proportional gain k_p should be well tuned to achieve good performance of the adaptive inverse compensation method, and can be established by assessing the results of numerical simulations of the real-time hybrid simulation that is to be performed.

Summary and Conclusions

Inherent servohydraulic dynamics in an actuator leads to actuator delay which has to be properly compensated to achieve reliable experimental results for a real-time hybrid simulation. An adaptive compensation method is proposed in this paper to achieve accurate actuator control using inverse compensation. An adaptive control law is developed for the compensation parameter using a TI that is based on the actuator tracking error. The compensation parameter is adapted to minimize the effect of inaccurately estimated and possibly time-varying actuator delay during a real-time hybrid simulation.

Laboratory tests involving real-time hybrid simulations of a SDOF MRF with an elastomeric damper are conducted to experimentally demonstrate the effectiveness of the proposed adaptive inverse compensation method. Different values of estimated actuator delay are used that include poor estimates representing an error in actuator delay of about 50% compared with the known amount of actuator delay. The tracking capability of the servohydraulic actuator is shown to be greatly improved and the actuator control error is significantly reduced when the adaptive inverse compensation method is used compared with the simulation results obtained using the conventional inverse compensation method. The proposed adaptive scheme is shown to require minimal information of the actuator delay before real-time hybrid simulation is performed, while enabling exceptional experimental results to be achieved.

The adaptive mechanism proposed in this paper can be generalized for other actuator delay compensation methods such as the linear acceleration method and the derivative feedforward method. Although the error TI is used for the adaptive mechanism, other forms of an error indicator, such as the hybrid simulation energy indicator, can also be adopted and incorporated into the adaptive inverse compensation method.

Acknowledgments

This paper is based upon work supported by grants from the Pennsylvania Department of Community and Economic Development through the Pennsylvania Infrastructure Technology Alliance, and by the National Science Foundation (NSF) under Grant No. CMS-0402490 within the George E. Brown, Jr. Network for Earthquake Engineering Testing Consortium Operation. Any opinions, findings, and conclusions expressed in this paper are those of the writers and do not necessarily reflect the views of the sponsors.

References

Ahmadizadeh, M., Mosqueda, G., and Reihorn, A. M. (2008). "Compensation of actuator delay and dynamics for real-time hybrid structural simulation." *Earthquake Eng. Struct. Dynam.*, 37(1), 21–42.

Bonnet, P. A., et al. (2007). "Real-time hybrid experiments with Newmark integration, MCSmd outer-loop control and multi-tasking strategies." *Earthquake Eng. Struct. Dynam.*, 36(1), 119–141.

Blakeborough, A., Williams, M. S., Darby, A. P., and Williams, D. M. (2001). "The development of real-time substructure testing." *Philos. Trans. R. Soc. London, Ser. A*, 359, 1869–1891.

Carrion, J. E., and Spencer, B. F. (2006). "Real-time hybrid testing using model-based delay compensation." *Proc., 4th Int. Conf. on Earthquake Engineering*, Taipei, Taiwan.

Chen, C. (2007). "Development and numerical simulation of hybrid effective force testing method." Ph.D. dissertation, Dept. of Civil and Environmental Engineering, Lehigh Univ., Bethlehem, Pa.

Chen, C., and Ricles, J. M. (2008a). "Development of direct integration algorithms for structural dynamics using discrete control theory." *J. Eng. Mech.*, 134(8), 676–683.

Chen, C., and Ricles, J. M. (2008b). "Stability analysis of direct integration algorithms applied to nonlinear structural dynamics." *J. Eng. Mech.*, 134(9), 703–711.

Chen, C., and Ricles, J. M. (2008c). "Stability analysis of SDOF real-time hybrid testing systems with explicit integration algorithms and actuator delay." *Earthquake Eng. Struct. Dynam.*, 37(4), 597–613.

Chen, C., Ricles, J. M., Marullo, T. and Mercan, O. (2009). "Real-time hybrid testing using the unconditionally stable explicit CR integration algorithm." *Earthquake Eng. Struct. Dynam.*, 38, 23–44.

Christenson, R., Lin, Y. Z., Emmons, A., and Bass, B. (2008). "Large-scale experimental verification of semi-active control through real-time hybrid simulation." *J. Struct. Eng.*, 134(4), 522–534.

Darby, A. P., Blakeborough, A., and Williams, M. S. (1999). "Real-time substructure tests using hydraulic actuators." *J. Eng. Mech.*, 125(10), 1133–1139.

Dermitzakis, S. N., and Mahin, S. A. (1985). "Development of substructuring techniques for on-line computer controlled seismic performance testing." *Rep. No. UBC/EERC-85/04*, Earthquake Engineering Research Center, Univ. of California, Berkeley, Berkeley, Calif.

Franklin, G. F., Powell, J. D., and Naeini, A. E. (2002). *Feedback control of dynamic systems*, 4th Ed., Prentice-Hall, Upper Saddle River, N.J.

Horiuchi, T., Inoue, M., Konno, T., and Namita, Y. (1999). "Real-time hybrid experimental system with actuator delay compensation and its application to a piping system with energy absorber." *Earthquake Eng. Struct. Dynam.*, 28(10), 1121–1141.

Horiuchi, T., and Konno, T. (2001). "A new method for compensating actuator delay in real-time hybrid experiment." *Philos. Trans. R. Soc. London, Ser. A*, 359, 1893–1909.

Jung, R. Y., and Shing, P. B. (2006). "Performance evaluation of a real-time pseudodynamic test system." *Earthquake Eng. Struct. Dynam.*, 35(7), 789–810.

Jung, R.Y., Shing, P. B., Stauffer, E., and Bradford, T. (2007). "Performance of a real-time pseudodynamic test system considering nonlinear structural response." *Earthquake Eng. Struct. Dynam.*, 36(12), 1785–1809.

Kontopanos, A. (2006). "Experimental investigation of a prototype elastomeric structural damper." MS thesis, Dept. of Civil and Environmental Engineering, Lehigh Univ., Bethlehem, Pa.

Lee, K. S., Fan, C. P., Sause, R., and Ricles, J. M. (2005). "Simplified design procedure for frame buildings with viscoelastic or elastomeric dampers." *Earthquake Eng. Struct. Dynam.*, 34(10), 1271–1284.

MATLAB. (2007). The MathWorks, Inc., Natick, Mass.

Mercan, O. (2007). "Analytical and experimental studies on large scale, real-time pseudodynamic testing." Ph.D. dissertation, Dept. of Civil and Environmental Engineering, Lehigh Univ., Bethlehem, Pa.

Mercan, O., and Ricles, J. M. (2007). "Stability and accuracy analysis of outer loop dynamics in real-time pseudodynamic testing of SDOF systems." *Earthquake Eng. Struct. Dynam.*, 36(11), 1523–1543.

Mercan, O., and Ricles, J. M. (2008). "NEES@Lehigh: Real-time hybrid pseudodynamic testing of large-scale structures." *Hybrid simulation: Theory, implementation and applications*, Chapter 10, V. Saouma and S. Mettupalayam, eds., Francis and Taylor, London.

Mosqueda, G., Stojadinovic, B., and Mahin, S. A. (2007a). "Real-time error monitoring for hybrid simulation. Part I: Methodology and experimental verification." *J. Struct. Eng.*, 133(8), 1100–1108.

Mosqueda, G., Stojadinovic, B., and Mahin, S. A. (2007b). "Real-time error monitoring for hybrid simulation. Part II: Structural response modification due to errors." *J. Struct. Eng.*, 133(8), 1109–1117.

Nakashima, M., Kato, H., and Takaoka, E. (1992). "Development of real-time pseudodynamic testing." *Earthquake Eng. Struct. Dynam.*, 21(1), 79–92.

Ogata, K. (1995). *Discrete-time control systems*, 2nd Ed., Prentice-Hall, Upper Saddle River, N.J.

Shao, X., Reinhorn, A. M., and Sivaselvan, M. (2006). "Real-time dynamic hybrid testing using force-based substructuring." *Proc., 2006 ASCE Structures Congress*, ASCE, Reston, Va.

Shing, P. B. (2002). "Development of high-speed on-line substructuring testing system at the University of Colorado." *Proc., CASCADE Technical Workshop*, Oxford, U.K.

Soong, T. T., and Spencer, B. F., Jr. (2002). "Supplemental energy dissipation: State-of-the-art and state-of-the-practice." *Eng. Struct.*, 24, 243–259.

Wallace, M. I., Sieber, J., Neild, S. A., Wagg, D. J., and Krauskopf, B. (2005a). "Stability analysis of real-time dynamic substructuring using delay differential equation models." *Earthquake Eng. Struct. Dynam.*, 34(15), 1817–1832.

Wallace, M. I., Wagg, D. J., and Neild, S. A. (2005b). "An adaptive polynomial based forward prediction algorithm for multi-actuator real-time dynamic substructuring." *Proc. R. Soc. London, Ser. A*, 461, 3807–3826.

Wen, Y. K. (1980). "Equivalent linearization for hysteretic systems under random excitation." *Trans. ASME, J. Appl. Mech.*, 47, 150–154.

Zhang, X. P., Ricles, J. M., Mercan, O., and Chen, C. (2005). "Servo-hydraulic system identification for the NEES real-time multi-directional earthquake simulation facility." *ATLSS Rep. No. 05-14*, Center for Advanced Technology for Large Structural Systems, Lehigh Univ., Bethlehem, Pa.

Zhao, J., French, C., Shield, C., and Posbergh, T. (2003). "Considerations for the development of real-time dynamic testing using servo-hydraulic actuation." *Earthquake Eng. Struct. Dynam.*, 32(11), 1773–1794.